Reconfigurable Power Divider enabled Dynamic Hybrid m-MIMO Transmitter

IEEE ComSoc IEEE Open Journal of the Communications Society

Dynamic Received XX Month XXXX; revised X Month XXXX; accepted XX Month XXXX. Date of publication XX Month XXXX; date of current version XX Month XXXX.

Digital Object Identifier 10.1109/OJCOMS.2020.1234567

Reconfigurable Power Divider enabled Dynamic Hybrid m-MIMO Transmitter

Kai Xu[1,2], Jiayu Hou[1], Li Wang[3], Simona Sibio[1], John S. Thompson[2], Steve McLaughlin[1], Yuan Ding[1], Gunnar Peters[3]

[1]School of Engineering and Physical Sciences, Heriot-Watt University, EH14 4AS, Edinburgh, UK
[2]Institute for Digital Communication, The University of Edinburgh, EH9 3JL, Edinburgh, UK
[3]R&D Center of Huawei Technologies, Sweden AB, Stockholm

CORRESPONDING AUTHOR: Kai Xu (e-mail: kx1@hw.ac.uk).

Yuan Ding's work was supported by the Engineering and Physical Sciences Research Council (EPSRC), UK, under grant number EP/V002635/1

ABSTRACT A promising solution for massive Multiple-Input Multiple-Output (m-MIMO) systems is Hybrid digital-analogue (HDA) beamforming as it offers a balanced trade-off between energy efficiency (EE) and spectral efficiency (SE). The lack of practical demonstrations in the open literature is primarily because those most existing works require a large number of phase shifters (PSs), radio frequency (RF) switches, power dividers (PDs), and power combiners which contribute to high hardware complexity and energy consumption (due to insertion loss). In this paper, we introduce a practical dynamic subarray m-MIMO structure that is based on reconfigurable power dividers (RPDs). The extensive system simulation results, considering hardware imperfection extracted from a practical RPD implementation, indicate that the proposed RPD-based dynamic HDA m-MIMO outperforms the fixed subarray counterpart.

INDEX TERMS Hybrid digital-analog beamforming, dynamic subarray, reconfigurable power dividers

I. INTRODUCTION

The proliferation of data and wireless devices demands higher capacity of wireless communication networks. Multiple-Input Multiple-Output (MIMO) has become a prevailing technology to significantly enhance the channel capacity by employing multiple antennas at both transmitter (Tx) and receiver (Rx) to explore multipath radio propagation channels. This high dimension of Tx and Rx propagation pairs creates an extra multiplexing domain, namely spatial multiplexing, in addition to the conventional time and frequency domains. In order for further channel capacity enhancement, the massive-MIMO (m-MIMO) concept [1],[2], where hundreds of antenna elements are equipped at Tx and/or Rx ends, is becoming a reality.

A major challenge of the m-MIMO architecture, as shown in Fig.1(a), is its high cost and complexity since every antenna is equipped with a dedicated radio frequency (RF) chain consisting of power-hungry power amplifiers, mixers, Digital-to-Analog Converters (DACs), etc. Furthermore, channel estimation, equalization, pre-coding, and baseband processing are all heavily burdens because of channel matrices of large dimensions. In order to alleviate this issue, various simplified m-MIMO architectures have been proposed in the literature [3]–[6]. They all follow the same concept, i.e., employing analog RF precoding networks (like power splitting, power combining, and phase shifting network or lens-based analog beamforming networks [7])to reduce the number of RF chains and thus the dimension of equivalent baseband channels. Hence, they are also labelled as hybrid digital-analog (HDA) m-MIMO.

In reference [8], a type of HDA m-MIMO structure, depicted in Fig. 1(b), was introduced. Here each RF chain, the number of which is less than the number of Tx antennas, is routed to all antennas via RF beamforming networks consisting of power dividers (PDs), power combiners, and phase shifters (PSs). This is commonly categorized as fully-connected HDA m-MIMO, which has been extensively investigated, for example in [9],[10]. The authors in [9] constructed an HDA beamformer by reducing the Euclidean distance between the HDA precoder and the optimal fully digital baseband precoder. By contrast, the HDA beamformer in [10] was designed using a codebook-based approach in which a series of analog precoders are pre-defined. The beamforming networks that enable this fully-connected m-MIMO, however, are still extremely complicated and costly when hardware implementation is considered, even with reducing the resolution of PSs [3],[10]–[14] or the resolution of DACs [15], [16].

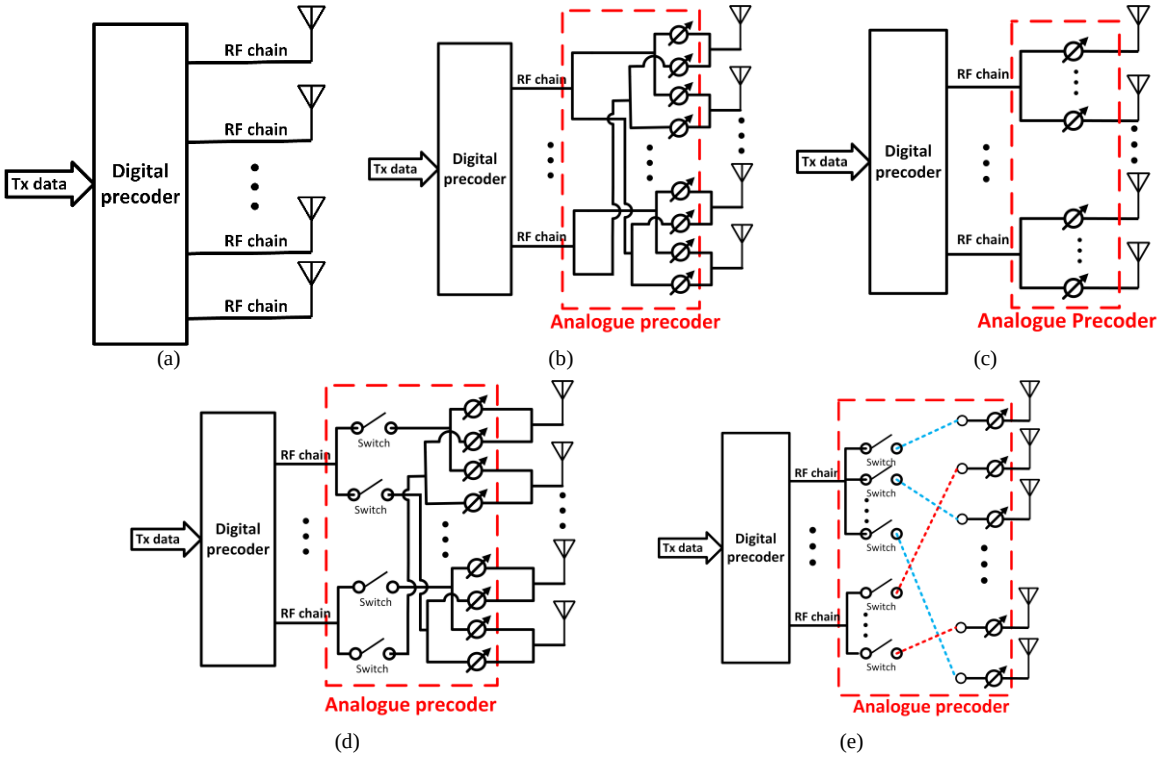

FIGURE 1. Various types of HDA m-MIMO architecture: a) fully digital; b) fully connected; c) fixed subarray; d) partially dynamic subarray; and e) fully dynamic subarray.

To further simplify required RF beamforming hardware another type of HDA structures was studied [5],[6],[17]–[25] named as partially-connected HDA m-MIMO, in which each RF chain is connected to a subset of the Tx antenna elements, referred to as a subarray. This partially-connected HDA m-MIMO can be sorted into two groups: To begin, the fixed subarray HDA structure [5],[6],[17],[18], as shown in Fig. 1(c), wherein the pairing of each RF chain and subarray is fixed. While the fixed subarray structure aims to maximize energy efficiency (EE) with reduced hardware complexity [19], it suffers low spectral efficiency (SE), especially in some dynamic propagation environments [20]. The reason for this is that low-resolution PSs and the reduced number of antennas in each subarray (compared with the full array) result in low precision on beam steering and low beamforming gain. The other category is the dynamic subarray HDA structure [18]–[25] which aims to strike a better trade-off between EE and SE. The dynamic subarray can be constructed with various degrees of reconfigurability of connecting RF chains and Tx antenna elements/subarrays. For example, in Fig. 1(d) a partially dynamic subarray [21],[22] allows each RF chain to dynamically connect to any subarrays where the antenna partition is fixed in each subarray. Alternatively, Fig. 1(e) shows a fully dynamic subarray [18],[19],[23],[24] that permits each RF chain to be adaptively linked to any arbitrary subset of the array antennas. The authors in [22],[23] developed an alternating-selection method by co-designing switching and phase-shifting networks with the objective to minimize the Euclidean distance between the ideal fully digital and HDA beamformers. In [25] the design of dynamic subarray beamformer was decoupled into two sub-problems for reduced computation complexity.

The majority of the dynamic subarray beamformer works discussed above, unfortunately, assume ideal RF components with little consideration of RF performance, insertion loss, and associated implementation cost, such as ideal mappers constructed using power dividers/combiners and/or switching networks [18],[19],[21]–[23]. And those reported structures require significantly more RF components for beamforming networks. More critically, the issue around impedance matching is not even considered. For example, in work [21] when a power combiner is used to combine power of signals from different RF chains of varied numbers, the power loss due to mismatch (or even matched) unused ports is not considered. These issues motivate us to construct a practical dynamic hybrid m-MIMO solution with low complexity and real hardware implementation. This will provide more in-depth insights into the impact of beamforming hardware candidates on the system performance

Under this context, in this work we study a practical dynamic subarray HDA m-MIMO that is constructed using two types of low-complexity reconfigurable PDs (RPDs) — power-ratio-tuneable RPDs (PT-RPDs) and port-selectable RPDs (PS-RPDs) — avoiding the use of lossy switching network, and low-resolution (3-bits) PSs with RF hardware imperfection involved. Two PS-RPD prototypes were designed, fabricated, and measured. Additionally, a PT-RPDs-assisted low-complexity algorithm for analog precoder designs are studied and evaluated for single-user (SU) m-MIMO and multi-user (MU) m-MIMO under various channel conditions. The results show that the 3-way PS-RPDs can consistently provide SNR gain of about 3.7 dB in both SU and

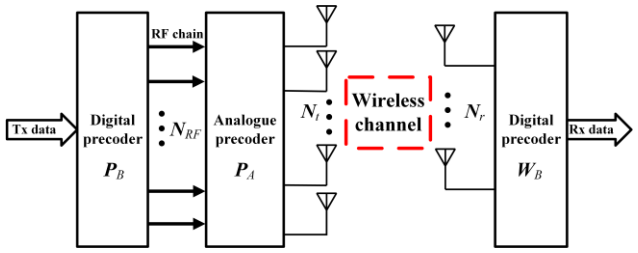

FIGURE 2. **Block diagram of HDA SU-MIMO system.**

MU m-MIMO system.

Notations: The following notations are used throughout this paper: Boldface upper-case and lower-case letters indicate matrices and vectors, respectively. Other lower-case letters represent coefficients or constants. $(\cdot)^T$, $(\cdot)^H$, $(\cdot)^{-1}$, $(\cdot)^\dagger$ and donate transpose, conjugate transpose, inversion, and Moore-Penrose pseudoinverse operations respectively. $\|\cdot\|$ is the Euclidean norm of a vector. E(·) and Var(·) refer to statistical expectation and variance. $\boldsymbol{I}_N$ represents an identity matrix with dimension N.

II. SYSTEM MODEL OF HDA m-MIMO, AND THE PROPOSED DYNAMIC SUBARRAY STRUCTURE

This section first discusses the generic HDA m-MIMO system model for SU and MU applications, followed by introducing our proposed dynamic subarray HDA m-MIMO based on RPDs

A. Hybrid Digital-Analog m-MIMO SYSTEM MODEL

SU-MIMO: In this sub-section, we present a SU-MIMO system with an HDA beamformer at Tx and a fully digital combiner at Rx as depicted in Fig. 2. Here it is assumed that the transmitter employs N_t antennas that are served by N_{RF} RF chains. N_s data streams are to be conveyed to a single receiver equipped with N_r Rx antennas and RF chains, where $N_s \leq N_r \leq N_{RF} < N_t$. At the transmitter side, as seen in Fig. 2, N_s data streams, denoted as $\boldsymbol{s} \in \mathbb{C}^{N_s \times 1}$, are first digitally precoded through the matrix $\boldsymbol{P}_B \in \mathbb{C}^{N_{RF} \times N_s}$ before being injected into N_{RF} RF chains. They are then up-converted to RF domain and further processed by an analog RF precoder $\boldsymbol{P}_A$. The excitation signal vector $\boldsymbol{x} \in \mathbb{C}^{N_t \times 1}$ at the Tx antenna array can thus be written as

$$\boldsymbol{x} = \boldsymbol{P}_A \boldsymbol{P}_B \boldsymbol{s}\,, \tag{1}$$

The digital precoder is power normalized, i.e., $\|\boldsymbol{P}_B\|^2 = 1$. Assuming that the wireless channel is assumed to be time-invariant, noted as $\boldsymbol{H} \in \mathbb{C}^{N_r \times N_t}$, the received baseband signal $\boldsymbol{y} \in \mathbb{C}^{N_s \times 1}$, after being processed through a digital baseband combiner $\boldsymbol{W}_B \in \mathbb{C}^{N_s \times N_r}$, becomes

$$\boldsymbol{y} = \boldsymbol{W}_B \boldsymbol{H} \boldsymbol{P}_A \boldsymbol{P}_B \boldsymbol{s} + \boldsymbol{n}\,, \tag{2}$$

where $\boldsymbol{n} \in \mathbb{C}^{N_s \times 1}$ is independently and identically distributed (i.i.d.) zero-mean complex Gaussian noise vector with a variance of σ^2.

Once the analog RF precoder $\boldsymbol{P}_A$ is designed, the digital baseband precoder $\boldsymbol{P}_B$ at the Tx end and the combiner matrix $\boldsymbol{W}_B$ at the Rx end can be obtained from the Singular Vector Decomposition (SVD) of the estimated effective channel matrix $\boldsymbol{H}_e$ of reduced dimension $\mathbb{C}^{N_r \times N_{RF}}$, see (3). The power allocation vector $\boldsymbol{\rho}$ can be found using water-filling on the singular value of the effective channel matrix.

$$\boldsymbol{H}_e = \boldsymbol{H}\boldsymbol{P}_A \tag{3}$$

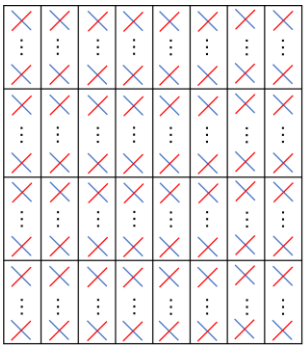

(a)

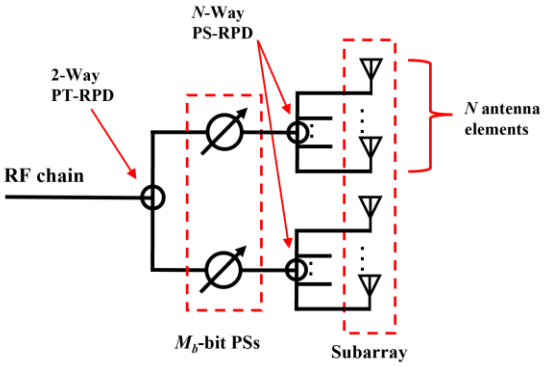

(b)

FIGURE 3. **a) A typical m-MIMO Tx full antenna panel [26]; b) Our proposed analog subarray precoding network.**

MU-MIMO: In the downlink MU-MIMO system, a base station (BS), which uses the same structure as that in the SU-MIMO, transmits signals to K users simultaneously. In order to eliminate the inter-user interference, linear precoding methods like channel inversion or Zero-forcing [27]–[29] can be adopted at transmitter end with a minimal level of complexity in baseband processing [29].

When each user in an MU-MIMO system is equipped with multiple receive antennas, it is feasible to transmit several parallel data streams to each user. In this scenario, the method of channel inversion, though workable, becomes inefficient since it essentially treats a user with a multiple antenna receiver as multiple independent users, each with a single receiving antenna. To tackle this issue, approaches like block channel inversion or block diagonalization are commonly used [27]. It allows transferring the transmit signal to be transferred to a group of antennas rather than a single antenna with zero-interference constraints. Here we use N_r^k to represent the number of receive antennas for user k out of a total of K users, and N_s^k as the corresponding number of

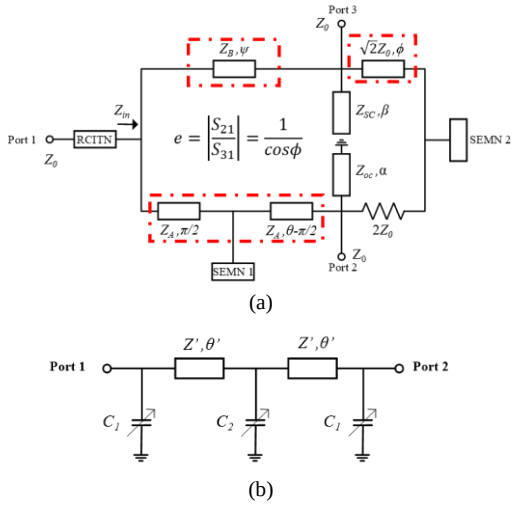

FIGURE 4. Diagrams of (a) 1-by-2 unequal power divider [30] and (b) tunable transmission line [31].

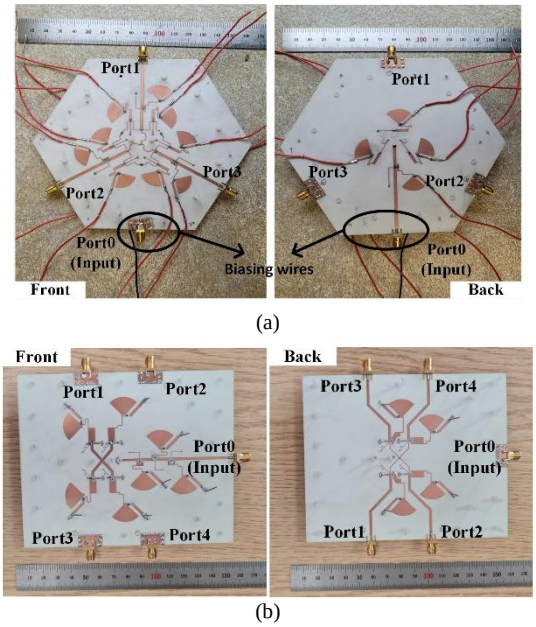

FIGURE 5. Photos of fabricated (a) 3-way and (b) 4-way PS-RPDs operating at 3.5 GHz with measured S-parameters presented in Appendix.

data streams for the same user. The received signals $\boldsymbol{y}_k$ for user k can be mathematically expressed as

$$\boldsymbol{y}_k = \boldsymbol{H}_k \boldsymbol{x} + \boldsymbol{n}_k = \boldsymbol{H}_k \boldsymbol{P}_A \boldsymbol{P}_B \boldsymbol{s} + \boldsymbol{n}_k, \tag{4}$$

where $\boldsymbol{H}_k \in \mathbb{C}^{N_r^k \times N_t}$ and $\boldsymbol{n}_k \in \mathbb{C}^{N_r^k \times 1}$ are, respectively, the channel matrix and associated noise for user k.

A combiner, as in the SU-MIMO scenario, is needed to post-process the received signals. When determining the baseband precoder and combiner using block diagonalization available to calculate the power allocation vector using water-filling method.

B.PROPOSED DYNAMIC SUBARRAY m-MIMO

Following the antenna structure reported in [26], in this paper we study a transmitter employing a planar antenna panel consisting of N_{RF} subarrays.

Each subarray consists of the same number of antenna elements with the size of $M_s = 2N$. In each subarray, there are N antennas for each orthogonal linear polarization, corresponding to red and blue elements in Fig. 3(a). Each subarray of $2N$ elements is excited with only one RF chain with the analog beamforming network comprised of a 2-way PT-RPD, two M_b-bit PSs, and two N-way PS-RPDs, see illustrations in Fig. 3(b).

The details on the two types of RPDs used in our proposed HRA m-MIMO transmitters are now explained.

2-way PT-RPD: The authors in [30] proposed a 2-way PD with unequal power division between output Ports 2 and 3, as illustrated in Fig. 4(a). And it also includes the special case of turning on or off one of the ports, achieved by two Switch Elements with Matching Networks (SEMNs) are added for port matching and selection, and one Reconfigurable Complex Impedance Transformer Network (RCITN) is inserted at input Port 1 for impedance matching. Readers are referred to [30] for more details. Since the power splitting ratio in this design is determined by the electrical lengths ψ, ϕ, θ, and the characteristic impedance Z_A, Z_B. Here we propose to replace these highlighted transmission lines in Fig. 4(a) with tunable ones described in [31] and depicted in Fig. 4(b) in order to reconfigure the power radio between Port 2 and Port 3. See equation (5)–(11) below. The p-i-n diodes MADP04230513060 from MACOM are used in our design simulation and implementation hereafter, and the varactor diode MA46H120 from MACOM is employed here for simulation.

$$\phi = arc\cos(\frac{1}{e}) \tag{5}$$

$$\theta = arc\cos(\sqrt{2}YZ_0\cos\phi - \sin\phi) \tag{6}$$

$$Z_A = \frac{\sqrt{2}Z_0\cos\phi}{\sin\theta} \tag{7}$$

$$\psi = \frac{\pi}{2} + arc\sin(\sqrt{2}YZ_0) \tag{8}$$

$$Z_B = \frac{\sqrt{2}Z_0}{\sin\psi} \tag{9}$$

$$C_1 = \frac{Z'(\cos 2\theta' - \cos\theta_{ttl}) + \cot\theta'(Z_{ttl}\sin\theta_{ttl} - Z'\sin 2\theta')}{\omega Z_{ttl} Z' \sin\theta_{ttl}} \tag{10}$$

$$C_2 = \frac{Z'\sin 2\theta' - Z_{ttl}\sin\theta_{ttl}}{\omega Z' Z' \sin^2\theta'} \tag{11}$$

where ω is angular frequency, characteristic impedance and electrical length of the tunable transmission line are Z_{ttl}, θ_{ttl} respectively.

N-way PS-RPD: The N-way PS-RPD introduced in [32] is able to control the 'On-Off' states of each output port using a switch-like component called SEMN which acts like a switch

but with a functionality to convert port impedance for matching. For the output ports in 'Off' state, the associated p-i-n diode is reverse-biased, and its parasitic inductance and capacitance are compensated through open and short-terminated microstrip stubs for enhanced port isolation. The power injected into these 'Off' ports is thus reflected back and re-routed to other ports in 'On' state, i.e., those with forward-biased diodes. This energy re-routing, however, alters the impedance of other ports. This issue is addressed by adding reconfigurable multiple-impedance transformer networks (RMITNs) at those ports. This RMITN is capable of transforming different load impedances into matched load impedance Z_0, through different combinations of forward and reverse biasing a set of p-i-n diodes. Thus, this N-way PS-RPD can greatly reduce the insertion loss. To facilitate system simulation in the next section, prototypes of 3-way and 4-way PS-RPDs are designed and fabricated, see Fig. 5, with all S-parameters at 3.5 GHz measured.

C. PROBLEM FORMULATION FOR PROPOSED DYNAMIC SUBARRAY HDA m-MIMO

In some previous works [9],[12], the HDA precoder design was formulated as finding solutions to minimizing the SE drop over fully digital systems. In SU-MIMO system this is written as in (12).

$$\{\boldsymbol{P}_A, \boldsymbol{P}_B\} = \arg\min_{\boldsymbol{P}_A, \boldsymbol{P}_B} \|\boldsymbol{P}_{FD} - \boldsymbol{P}_A \boldsymbol{P}_B\|, \quad s.t. \begin{cases} \|\boldsymbol{P}_B\|^2 = 1 \\ \boldsymbol{P}_A \in \mathcal{P} \end{cases} \tag{12}$$

Here $\boldsymbol{P}_{FD}$ is the ideal precoder in fully digital MIMO systems. $\|\boldsymbol{P}_B\|^2 = 1$ is added for power normalization, while $\mathcal{P}$ is a set representing the phase and modulus constraints determined by the analog beamforming network, In the proposed system studied in this paper, the precoder consists of M_b-bits PSs and two types of RPDs. However, in practical HDA m-MIMO systems not all entries of $\boldsymbol{P}_{FD}$ can be measured, because there are only limited number of RF chains. Therefore, the HDA precoder design problem is instead formulated to maximizing system SE as in (13).

$$\{\boldsymbol{P}_A, \boldsymbol{P}_B\} = \arg\max_{\boldsymbol{P}_A, \boldsymbol{P}_B} \sum \log_2 \left| \boldsymbol{I} + \frac{\boldsymbol{W}_B \boldsymbol{H} \boldsymbol{P}_A \boldsymbol{P}_B \boldsymbol{P}_B' \boldsymbol{P}_A' \boldsymbol{H}' \boldsymbol{W}_B}{\sigma_N^2} \right|, \quad s.t. \begin{cases} \|\boldsymbol{P}_B\|^2 = 1 \\ \boldsymbol{P}_A \in \mathcal{P} \end{cases} \tag{13}$$

Here $\boldsymbol{HP}_A$, as discussed in (3), can be replaced by an effective channel matrix $\boldsymbol{H}_e$, and the digital baseband precoder $\boldsymbol{P}_B$ and baseband combiner $\boldsymbol{W}_B$ can subsequently be derived from the decomposition of the effective channel $\boldsymbol{H}_e$ using SVD.

$$\begin{cases} \boldsymbol{H}_e = \boldsymbol{U}_e \boldsymbol{\lambda}_e \boldsymbol{V}_e' \\ \boldsymbol{P}_B = \sqrt{\boldsymbol{\rho}} \boldsymbol{V}_e \\ \boldsymbol{W}_B = \boldsymbol{U}_e' \end{cases} \tag{14}$$

In (14) $\boldsymbol{\lambda}_e \in \mathbb{C}^{\min(N_{RF}, N_r) \times \min(N_{RF}, N_r)}$ is a diagonal singular matrix, $\boldsymbol{V}_e$ and $\boldsymbol{U}_e$ are left and right singular matrices, respectively. Note that the power allocation vector $\boldsymbol{\rho}$ is obtained by applying the water-filling algorithm to $\boldsymbol{\lambda}_e$. It is worth emphasizing that they are also unitary matrices, indicating that they will not affect the value of the objective function in (13). With (14), the formulation in (13) can be simplified into (15).

$$\{\boldsymbol{P}_A, \boldsymbol{P}_B\} = \arg\max_{\boldsymbol{P}_A, \boldsymbol{P}_B} \sum \log_2 \left| \boldsymbol{I} + \frac{\boldsymbol{\rho} \boldsymbol{\lambda}_e \boldsymbol{\lambda}_e'}{\sigma_N^2} \right| \tag{15}$$

Therefore, the optimization problem in (15) is equivalent to finding an optimal RF precoder to maximize the sum of squared singular values of the effective channel matrix, see (16),

$$\boldsymbol{P}_A = \arg\max \sum \ell^2(\boldsymbol{H}_e) = \arg\max \sum \ell^2(\boldsymbol{H}\boldsymbol{P}_A), \quad s.t. \quad \boldsymbol{P}_A \in \mathcal{P} \tag{16}$$

where $\boldsymbol{\ell}(\cdot)$ denotes SVD operation which returns singular values of the enclosed matrix.

The algorithm to find the optimal RF precoder will be introduced in the following section. There the configurations of N-way PS-RPDs are first determined using an iteration method with the criterion to maximize the received signal power. Then the channel covariance matrix [18],[33] approach is employed to determine the settings of the 2-way PT-RPDs and quantized PSs.

In MU-MIMO scenarios the design problem can be regarded as a combination of several independent SU-MIMO systems but using different baseband precoding methods to manage inter-user interference and maximize the sum rate.

III. DESIGN ALGORITHMS FOR THE PROPOSED DYNAMIC SUBARRAY HDA m-MIMO

In this section, the algorithms for implementing (16) are described and which find optimal settings for two types of RPDs and M_b-bit PSs.

The design of the analog precoder in Fig. 3(b) in the dynamic subarray can be separated into two subproblems: (i) searching for the optimal antenna combination in each subarray and (ii) determining the low-resolution PSs and 2-way PT-RPDs output power ratios among two polarization sections. The methods we use in our work to tackle these two subproblems are summarized as below, and it is assumed that the full channel matrix $\boldsymbol{H}$ is unknown to both Tx and Rx.

Antenna Combination Selection: The reconfigurability here is employed to control the 'On-Off' states of the output ports

Algorithm 1 Covariance matrix method of determining power splitting ratio and phase shifting

Preparation:
Y: Received signals at BS over T snapshots when the user transmits pilot signals of all ones
A: Tx antenna array response matrix (beam steering in different Angles of Arrival)
L: Estimated number of wireless channel paths

Input: $\boldsymbol{\Phi}$, $\boldsymbol{Y}$, L, $\boldsymbol{A}$
Initialization: $\boldsymbol{R}_y = \boldsymbol{Y}\boldsymbol{Y}^H/T$, $\boldsymbol{V} = \boldsymbol{R}_y$, $S = \boldsymbol{\Phi}$
1: **for** $n = 1 : L$ **do**
2: $j = \arg\max_i |[\boldsymbol{\Phi}]^H_{:,i} \boldsymbol{V} [\boldsymbol{\Phi}]_{:,i}|$
3: $S = S \cup \{ j \}$
4: $\boldsymbol{R}_{\hat{g}} = [\boldsymbol{\Phi}]^{\dagger}_{:,S} \boldsymbol{R}_y ([\boldsymbol{\Phi}]^{\dagger}_{:,S})^H$
5: $\boldsymbol{V} = \boldsymbol{V} - [\boldsymbol{\Phi}]_{:,S} \boldsymbol{R}_{\hat{g}} [\boldsymbol{\Phi}]^H_{:,S}$
6: **end for**
7: $\boldsymbol{R} = \boldsymbol{A}\boldsymbol{R}_{\hat{g}}\boldsymbol{A}^H$
8: 2-way PT-RPDs e^2 can be calculated via (19)
9: Phase shifting can be calculated via $\max(\boldsymbol{\ell}(\boldsymbol{R}_{sr}))$

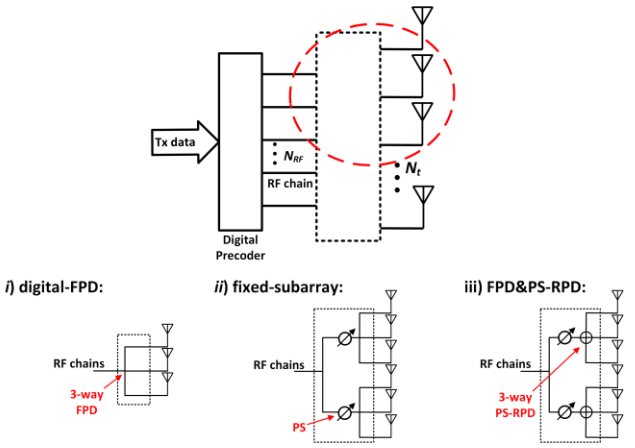

FIGURE 6. Benchmarking Tx architectures, taking N = 3 as an example.

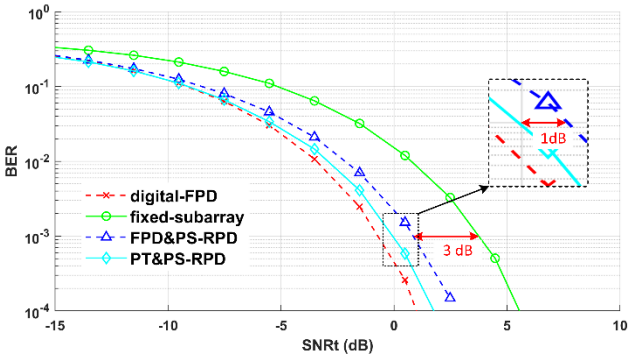

FIGURE 7. Simulated BER curves of the proposed 2-way PT-RPDs and 3-way PS-RPDs based dynamic subarray SU-MIMO (PT&PS-RPD) against other benchmarking systems.

in N-way PS-RPDs in order to allocate more signal power to the antenna element(s) that have lower channel loss to the targeted Rx. When considering exhaustive search method to experience all combinations, the iteration space needed for $2\times N_{RF}$ N-way PS-RPDs is of size $(2^N - 1)^{2\times N_{RF}}$. For example, when $N = 3$ and $N_{RF} = 32$, the total iteration would be over 10^{54}, making this exhaustive search method infeasible. While it is found that the use of 2-way PT-RPDs can make each antenna subarray be optimized independently. Thus, this reduces the search space to $(2^N - 1)\times 2\times N_{RF}$. For the same example, the size of the iteration space dramatically drops to 448. With the help of Rx feedback, each N-way PS-RPD configuration corresponding to the maximum Rx signal power can be identified. The essence that these N-way PS-RPDs can be treated independently is that the signal magnitudes and phases can be further adjusted by the remaining 2-way PT-RPDs and PSs in-between.

Power Splitting and Phase Shifting between Two antenna Sections in Subarrays: Author Sungwoo proposed the channel covariance matrix method to design analog precoders in [18], summarized in Algorithm 1. Here the largest singular value of the channel covariance matrix is used to determine the values of PSs in a fixed subarray structure, where each RF chain connects to M_s antennas via M_s PSs. In our dynamic subarray structure, after determining the N-way PS-RPDs, the subset of each subarray is fixed as well. Therefore, the channel covariance matrix method can also be used to determine the values of PSs when the number of paths in the wireless channel is roughly known. The detailed method to estimate the channel covariance is described in [33]. When applying the channel covariance estimation method in our work, the 2-way PT-RPDs are set up as the equal power mode, and the N-way PS-RPDs are configured with optimal setting obtained in the first step. The next step is to determine the power ratio e^2 of the 2-way PT-RPDs. Recall the definition of the channel covariance matrix [33], and re-write it in (17),

$$\boldsymbol{R} = \boldsymbol{H}\boldsymbol{H}^H = \begin{pmatrix} \boldsymbol{h}_{1,1} & \cdots & \boldsymbol{h}_{1,N_r} \\ \vdots & \ddots & \vdots \\ \boldsymbol{h}_{N_t,1} & \cdots & \boldsymbol{h}_{N_t,N_r} \end{pmatrix} \times \begin{pmatrix} \boldsymbol{h}^H_{1,1} & \cdots & \boldsymbol{h}^H_{1,N_r} \\ \vdots & \ddots & \vdots \\ \boldsymbol{h}^H_{N_t,1} & \cdots & \boldsymbol{h}^H_{N_t,N_r} \end{pmatrix} \quad (17)$$

from which the diagonal elements in $\boldsymbol{R}$ can be extracted as in (18).

$$\begin{aligned} \boldsymbol{R}_{dia1} &= \boldsymbol{h}_{1,1}\boldsymbol{h}^H_{1,1} + \boldsymbol{h}_{1,2}\boldsymbol{h}^H_{1,2} + \cdots + \boldsymbol{h}_{1,N_r}\boldsymbol{h}^H_{1,N_r} \\ &\vdots \\ \boldsymbol{R}_{diaN_t} &= \boldsymbol{h}_{N_t,1}\boldsymbol{h}^H_{N_t,1} + \boldsymbol{h}_{N_t,2}\boldsymbol{h}^H_{N_t,2} + \cdots + \boldsymbol{h}_{N_t,N_r}\boldsymbol{h}^H_{N_t,N_r} \end{aligned} \quad (18)$$

Each diagonal element can be regarded as the path gain associated with the corresponding transmit antenna. The concept of finding optimal settings for the 2-way PT-RPDs is similar to the water-filling algorithm when determining the power allocation vector $\boldsymbol{\rho}$. The power ratio of the 2-way PT-RPDs e^2 can thus be computed as

$$e^2_{sr} = \frac{\text{sum}(\boldsymbol{R}_{diaS_{r,a1}})}{\text{sum}(\boldsymbol{R}_{diaS_{r,a2}})} \quad \text{for} \quad r = 1, 2, \cdots, N_{RF}, \quad (19)$$

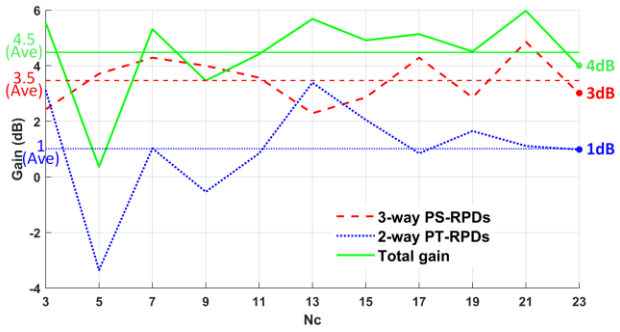

FIGURE 8. SNR gains obtained from the 2-way PT-RPDs and the 3-way PS-RPDs for different N_c in SU m-MIMO.

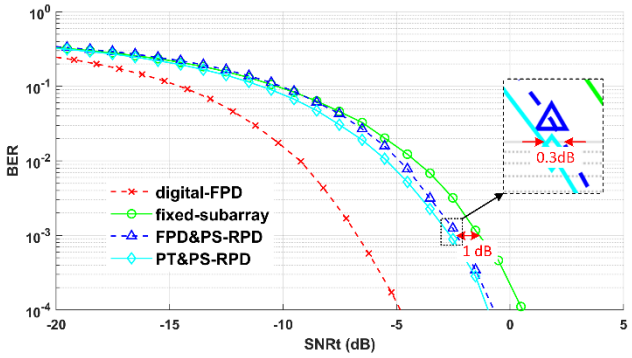

FIGURE 9. Simulated BER curves of the proposed 2-way PT-RPDs and 4-way PS-RPDs based dynamic subarray SU m-MIMO (PT&PS-RPD) against other benchmarking systems.

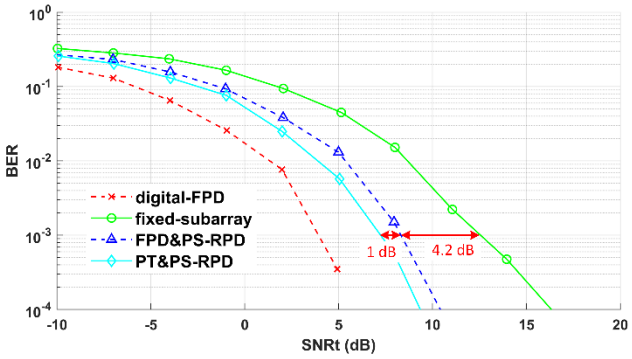

FIGURE 10. Simulated BER curves of the proposed 2-way PT-RPDs and 3-way PS-RPDs based dynamic subarray MU m-MIMO (PT&PS-RPD) against other benchmarking systems.

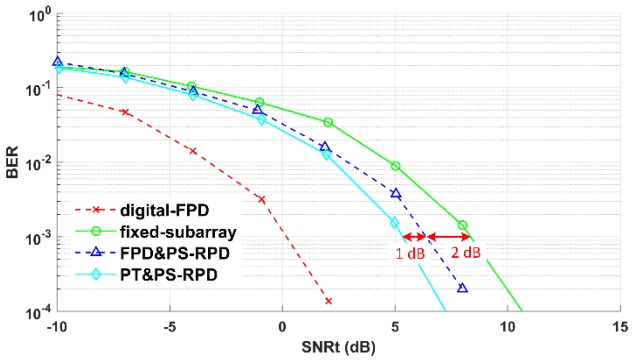

FIGURE 11. Simulated BER curves of the proposed 2-way PT-RPDs and 4-way PS-RPDs based dynamic subarray MU m-MIMO (PT&PS-RPD) against other benchmarking systems

TABLE 1 Average SNR gains (in dB) contributed by different types of RPDs in SU and MU m-MIMO systems

	PT-PS-RPD (N = 3)			PT-PS-RPD (N = 4)		
	PT-RPD	PS-RPD	Total	PT-RPD	PS-RPD	Total
SU	1	3.5	4.5	0.3	1.5	1.8
MU	1	3.9	4.9	0.1	1.8	1.9

where $\boldsymbol{R}_{diaS_{r,a\{1,2\}}}$ is the diagonal element of channel covariance matrix associated with the antenna section connected with the {1st, 2nd} output port of the 2-way PT-RPD in the r^{th} subarray.

After obtaining the optimal settings of PSs, 2-way PT-RPDs and N-way PS-RPDs, the analog precoder can be constructed. The baseband precoder and combiner can then be derived using (14).

IV. SYSTEM PERFORMANCE EVALUATION

In this section, the simulation results are presented to evaluate the performance of our proposed RPDs-based dynamic subarray HDA m-MIMO.

In the simulation, the CDL-B wireless channel model [34] is employed with the number of paths $L = N_c \times M_r$ where N_c is number of clusters and M_r of 20 is the number of rays in each cluster. The system simulation is performed at 3.5 GHz and Orthogonal Frequency Division Multiplexing (OFDM) signals with 64 subcarriers of 15 kHz spacing are used. The data streams, where $N_s = 2$ for each user, are Quadrature Phase Shift Keying (QPSK) modulated in each subcarrier. In our system simulation, we assume PSs are 3-bit with 0.5 dB insertion loss, and the insertion loss for N-way fixed power dividers (FPDs) are 1 dB when $N = 3$ and 1.2 dB when $N = 4$, which are typical performance of some commercial devices, e.g. ZB3PD-63+ and ZN4PD1-63HP-S+ from Mini-Circuits. Measured S-parameters of N-way PS-RPDs are used in the link simulation. The 2-way PT-RPD is simulated in ADS with practical lossy diodes and lossy dielectric materials included.

A. BER PERFORMANCE ANALYSIS

Firstly, the SU m-MIMO system is considered to evaluate the performance of our proposed dynamic subarray HDA beamformer (labelled as PT&PS-RPD), depicted in Fig. 3(b). For performance comparison and to reveal the benefits of those RPDs, we also simulate the systems with the following beamforming structures (taking $N = 3$ as an example): *i*) 64 RF chains, each of which connects to a 3-element Tx subarray via a 3-way FPD (labelled as digital-FPD); *ii*) 32 RF chains, each of which connects to a 6-element Tx subarray via a 2-way fixed PD, PSs, and two 3-way fixed PDs (labelled as fixed-subarray); and finally *iii*) 32 RF chains, each of which connects to a 6-element Tx subarray via a 2-way fixed PD, PSs, and two 3-way PS-RPDs (labelled as FPD&PS-RPD). These benchmarking Tx architectures are illustrated in Fig. 6.

Following the design procedures and algorithms described in Section 3, the simulated bit error rate (BER) curves versus SNR_t (signal to noise ratio normalized at Tx end) for the proposed 2-way PT-RPDs and 3-way PS-RPDs based dynamic subarray SU m-MIMO (namely PT&PS-RPD)

against other benchmarking systems introduced above are depicted in Fig. 7. The CDL-B channel with 23 clusters (N_c = 23) is assumed in the simulation. It can be observed that the proposed dynamic subarray PT&PS-RPD outperforms the fixed-subarray by 4 dB, in which the 3-way PS-RPDs and the 2-way PT-RPD contribute to 3 dB and 1 dB respectively. Here the gain in this section is defined as the gap in SNR_t when BER equals 10^{-3}, seen in Fig. 7. When considering different channel conditions, for example different number of clusters N_c, the total SNR gains obtained, compared with the fixed-subarray system, as well as gains contributed by the 3-way PS-RPDs and 2-way PT-RPD, are plotted in Fig. 8. In average 4.5 dB gain can be achieved. It is also important to highlight that with half number of RF chains the proposed dynamic subarray only compromises less than 1 dB SNR when comparing with the corresponding digital-FPD system. When the antenna panel is extended from 192 antenna elements to 256 elements, the 4-way PS-RPDs, see the prototype in Fig. 5(b), can be employed to keep the number of RF chains unchanged. Fig. 9 shows BER curve versus SNR_t for the 2-way PT-RPD and 4-way PS-RPDs based dynamic subarray SU m-MIMO system under CDL-B channel with N_c = 23. The results in Fig. 9 show that the overall achievable gain is reduced from 4 dB to 1.5 dB, and, in particular, the gain provided by the 2-way PT-RPD diminishes by comparing FPD&PS-RPD BER curve with PT&PS-RPD.

In MU m-MIMO systems, the similar conclusion can be obtained, see simulation results for 192 antennas (with 3-way PS-RPDs) and 256 antennas (with 4-way PS-RPDs) in Fig. 10 and Fig. 11.

The SNR gains from RPDs in both SU and MU m-MIMO systems are averaged over different channel condition (NO. clusters) and are summarized in Table 1. Overall, *N*-way PS-RPDs deliver more performance improvement than 2-way PT-RPDs, while the m-MIMO system benefits at least 2 dB more gain from 3-way PS-RPDs than 4-way PS-RPDs.

To demonstrate performance gain from our proposed dynamic structure, the comparison with the peer's work is carried out. However, the existing dynamic HDA m-MIMO structures [18],[19],[21]–[23] have issues in their complex beamforming networks and the lack of information on the performance of employed RF components, such as insertion loss, impedance matching, etc. Among those reported HAD m-MIMO candidates, a few assumptions are made to compare their performance to our proposed system. For example, the one employed for multi-user/multi-cellular system in [35], re-drawn in Fig. 12, is constructed, in each RF chain, using a 6-way power divider, 6 switches, and 6 antennas. This is the counterpart for our proposed solution when N = 3. Here we assume the insertion loss of the switches is 0.5 dB, and that of 6-way power dividers is 2 dB. The BER simulation results are presented in Fig. 13, to compare the performance of our proposed PT&PS-RPD against this adaptive beamformer in [35], and fixed subarray. There is around 2.3 dB performance gain available from our proposed dynamic structure.

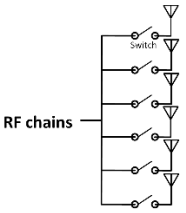

FIGURE 12. Adaptive beamformer structure in each RF chain proposed in [35].

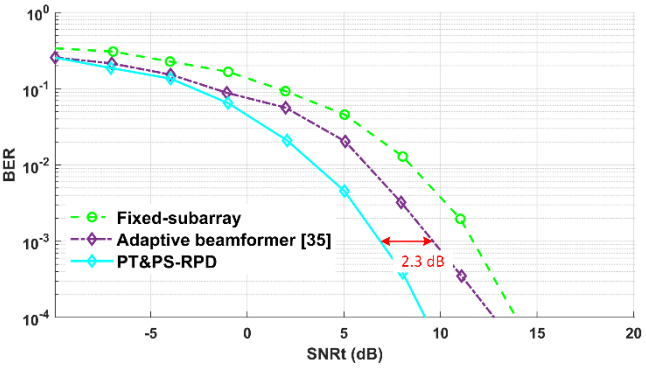

FIGURE 13. Simulated BER curves of the proposed 2-way PT-RPDs and 3-way PS-RPDs based dynamic subarray MU m-MIMO (PT&PS-RPD) against the adaptive beamformer and fixed subarray structures.

TABLE 2. Hardware complexity analysis represented by the number of RF components and control signals required in each RF chain.

Dynamic Structure	Type of PDs/PCs	No. switches	No. 3-bit PSs	No. control signals
[18, 19, 23]	192-way PD 192-way PC	192	6	210*
[21, 22]	32-way PD 32-way PC	32	192	608*
[35]	6-way PD	6	0	6*
Our proposed	2-way PT-RPD 3-way PS-RPD	0	6	34*,12#

* Indicating digital control signals; # Indicating analog control signals

B.HARDWARE COMPLEXITY ANALYSIS

The energy consumption of the analog beamformers we used is tiny, in the order of microwatt, since only p-i-n and varactor diodes were exploited for reconfigurability. Thus, this energy consumption, comparing with tens or even hundreds of W consumed by RF chains, can be safely ignored. However, the complexity of the employed beamforming networks comes from the number of signals required for control/reconfiguration.

Here the hardware complexity is analyzed and quantized with regard to the number of control signals required by analog beamformers associated with a single RF chain. For our proposed structure, there exist one 2-way PT-RPD of 15 control signals (12 analog signals and 3 digital signals), two *N*-way PS-RPDs of (3*N*–1) digital control signals each, and two 3-bit PSs (3 digital control signals per PS). For an antenna panel of 192 Tx antennas (N = 3), a total of 34 digital and 12 analog control signals are needed. While for the structure

using ideal mappers [18],[19],[21]–[23] , each RF chain requires power dividers (PDs) and power combiners (PCs) with much greater number of ports, e.g., 192-way for those in [18],[19],[23], and 32-way for those in [21],[22]. A practical structure called adaptive beamformer [35] employs only one 6-way PD and 6 switches for each RF chain output. A detailed complexity comparison against some reported dynamic hybrid m-MIMO structures is presented in Table 2.

V.CONCLUSION

In this paper, we proposed a novel and practical dynamic subarray HDA m-MIMO beamforming structure which is realized by two types of RPDs (PT-RPDs and PS-RPDs) and 3-bit PSs. The extensive system simulation results, considering hardware imperfection extracted from practical RPD implementation, indicate that the proposed RPD-based dynamic HDA m-MIMO outperforms the fixed subarray counterpart. For instance, a 4.9 dB SNR gain was obtained in MU m-MIMO system which was constructed with 2-way PT-RPDs and 3-way PS-RPDs.

APPENDIX

TABLE 3. Measured S-Parameters of the 4-way RPD shown in Fig. 5(b).

	States*	S_{10} (dB)	S_{20} (dB)	S_{30} (dB)	S_{40} (dB)
Mode 1	(1)	–1.50	–26.99	–23.72	–25.78
	(2)	–23.46	–1.54	–23.85	–25.35
	(3)	–23.97	–26.28	–1.55	–26.95
	(4)	–23.81	–25.80	–23.51	–1.55
Mode 2	(1,2)	–4.59	–4.74	–26.85	–27.50
	(1,3)	–4.66	–28.46	–4.47	–28.10
	(1,4)	–4.53	–28.17	–26.41	–4.58
	(2,3)	–26.78	–4.78	–4.40	–27.80
	(2,4)	–27.12	–4.68	–26.92	–4.54
	(3,4)	–26.98	–27.57	–4.48	–4.75
Mode 3	(1,2,3)	–6.45	–6.62	–6.05	–30.82
	(1,2,4)	–6.27	–6.58	–27.65	–6.23
	(1,3,4)	–6.30	–30.84	–6.20	–6.43
	(2,3,4)	–28.39	–6.47	–6.06	–6.49
Mode 4	(1,2,3,4)	–7.60	–7.86	–7.52	–7.71

*Indices of activated output ports

TABLE 4. Measured S-Parameters of the 3-way RPD shown in Fig. 5(a).

	States*	S_{10} (dB)	S_{20} (dB)	S_{30} (dB)
Mode 1	(1)	–2.31	–29.41	–28.74
	(2)	–27.57	–2.47	–28.17
	(3)	–28.10	–29.14	–2.52
Mode 2	(1,2)	–4.42	–4.42	–30.72
	(1,3)	–4.43	–31.3	–4.53
	(2,3)	–29.86	–4.51	–4.56
Mode 3	(1,2,3)	–5.72	–5.63	–5.76

*Indices of activated output ports

REFERENCES

[1] T. L. Marzetta, "Noncooperative Cellular Wireless with Unlimited Numbers of Base Station Antennas," *IEEE Trans. Wirel. Commun.*, vol. 9, no. 11, pp. 3590–3600, November 2010, DOI: 10.1109/TWC.2010.092810.091092.

[2] J. Hoydis, S. ten Brink, and M. Debbah, "Massive MIMO: How Many Antennas Do We Need?" *2011 49th Annu. Allerton Conf. Commun. Control Comput. (Allerton)*, 2011, pp. 545–550, DOI: 10.1109/Allerton.2011.6120214.

[3] A. Alkhateeb, G. Leus, and R. W. Heath, "Limited Feedback Hybrid Precoding for Multi-User Millimeter Wave Systems," *IEEE Trans. Wirel. Commun.*, vol. 14, no. 11, pp. 6481–6494, Nov. 2015, DOI: 10.1109/TWC.2015.2455980.

[4] F. Sohrabi and W. Yu, "Hybrid Digital and Analog Beamforming Design for Large-Scale Antenna Arrays," *IEEE J. Sel. Top. Signal Process.*, vol. 10, no. 3, pp. 501–513, April 2016, DOI: 10.1109/JSTSP.2016.2520912.

[5] X. Gao, L. Dai, S. Han, C. -L. I, and R. W. Heath, "Energy-Efficient Hybrid Analog and Digital Precoding for MmWave MIMO Systems with Large Antenna Arrays," *IEEE J. Sel. Areas Commun.*, vol. 34, no. 4, pp. 998–1009, April 2016, DOI: 10.1109/JSAC.2016.2549418.

[6] J. Deng, O. Tirkkonen, and C. Studer, "MmWave Multiuser MIMO Precoding with Fixed Subarrays and Quantized Phase Shifters," *IEEE Trans. Veh. Technol.*, vol. 68, no. 11, pp. 11132–11145, Nov. 2019, DOI: 10.1109/TVT.2019.2944224.

[7] Y. Ding, V. Fusco, A. Shitvov, Y. Xiao and H. Li, "Beam Index Modulation Wireless Communication With Analog Beamforming," *IEEE Trans. Veh. Technol.*, vol. 67, no. 7, pp. 6340–6354, July 2018, doi: 10.1109/TVT.2018.2819728.

[8] Z. Pi and F. Khan, "An introduction to millimeter-wave mobile broadband systems," *IEEE Commun. Mag.*, vol. 49, no. 6, pp. 101–107, June 2011, DOI: 10.1109/MCOM.2011.5783993.

[9] X. Yu, J. -C. Shen, J. Zhang, and K. B. Letaief, "Alternating Minimization Algorithms for Hybrid Precoding in Millimeter Wave MIMO Systems," *IEEE J. Sel. Top. Signal Process.*, vol. 10, no. 3, pp. 485–500, April 2016, DOI: 10.1109/JSTSP.2016.2523903.

[10] S. Said, W. Saad, and M. Shokair, "MMSE Algorithm Based Two Stages Hybrid Precoding for Millimeter Wave Massive MIMO Systems," *Analog Integr Circ Sig Process 98*, pp. 565–573, Oct. 2019, DOI:10.1007/s10470-018-1354-7.

[11] L. Liang, W. Xu, and X. Dong, "Low-Complexity Hybrid Precoding in Massive Multiuser MIMO Systems," *IEEE Commun. Lett.*, vol. 3, no. 6, pp. 653–656, Dec. 2014, DOI: 10.1109/LWC.2014.2363831.

[12] J. -C. Chen, "Hybrid Beamforming with Discrete Phase Shifters for Millimeter-Wave Massive MIMO Systems," *IEEE Trans. Veh. Technol.*, vol. 66, no. 8, pp. 7604–7608, Aug. 2017, DOI: 10.1109/TVT.2017.2670638.

[13] W. Tan, M. Matthaiou, S. Jin, and X. Li, "Spectral Efficiency of DFT-Based Processing Hybrid Architectures in Massive MIMO," *IEEE Commun. Lett.*, vol. 6, no. 5, pp. 586–589, Oct. 2017, DOI: 10.1109/LWC.2017.2719036.

[14] W. Tan, D. Xie, J. Xia, W. Tan, L. Fan, and S. Jin, "Spectral and Energy Efficiency of Massive MIMO for Hybrid Architectures Based on Phase Shifters," *IEEE Access*, vol. 6, pp. 11751–11759, 2018, DOI: 10.1109/ACCESS.2018.2796571.

[15] A. Kaushik, E. Vlachos, C. Tsinos, J. Thompson and S. Chatzinotas, "Joint Bit Allocation and Hybrid Beamforming Optimization for Energy Efficient Millimeter Wave MIMO Systems," *IEEE Trans. Green Commun. Netw.*, vol. 5, no. 1, pp. 119-132, March 2021, doi: 10.1109/TGCN.2020.3026725.

[16] E. Vlachos and J. Thompson, "Energy-Efficiency Maximization of Hybrid Massive MIMO Precoding With Random-Resolution DACs via RF Selection," *IEEE Trans. Wirel. Commun.*, vol. 20, no. 2, pp. 1093-1104, Feb. 2021, doi: 10.1109/TWC.2020.3030772.

[17] M. Li, Z. Wang, H. Li, Q. Liu, and L. Zhou, "A Hardware-Efficient Hybrid Beamforming Solution for mmWave MIMO Systems," *IEEE Wirel. Commun.*, vol. 26, no. 1, pp. 137–143, February 2019, DOI: 10.1109/MWC.2018.1700391.

[18] S. Park, A. Alkhateeb, and R. W. Heath, "Dynamic Subarrays for Hybrid Precoding in Wideband mmWave MIMO Systems," *IEEE Trans. Wirel. Commun.*, vol. 16, no. 5, pp. 2907–2920, May 2017, DOI: 10.1109/TWC.2017.2671869.

[19] H. Li, M. Li, and Q. Liu, "Hybrid Beamforming With Dynamic Subarrays and Low-Resolution PSs for mmWave MU-MISO Systems," *IEEE Trans Commun*, vol. 68, no. 1, pp. 602–614, Jan. 2020, DOI: 10.1109/TCOMM.2019.2950905.

[20] X. Gao, L. Dai, Y. Sun, S. Han, and I. Chih-Lin, "Machine learning inspired energy-efficient hybrid precoding for mmWave massive MIMO systems," *2017 IEEE International Conference on Communications (ICC)*, 2017, pp. 1–6, DOI: 10.1109/ICC.2017.7997065.
[21] L. Yan, C. Han, and J. Yuan, "A Dynamic Array-of-Subarrays Architecture and Hybrid Precoding Algorithms for Terahertz Wireless Communications," *IEEE J. Sel. Areas Commun.*, vol. 38, no. 9, pp. 2041–2056, Sept. 2020, DOI: 10.1109/JSAC.2020.3000876.
[22] F. Yang, J. -B. Wang, M. Cheng, J. -Y. Wang, M. Lin, and J. Cheng, "A Partially Dynamic Subarrays Structure for Wideband mmWave MIMO Systems," *IEEE Trans Commun*, vol. 68, no. 12, pp. 7578–7592, Dec. 2020, DOI: 10.1109/TCOMM.2020.3020833.
[23] H. Li, M. Li, Q. Liu, and A. L. Swindlehurst, "Dynamic Hybrid Beamforming with Low-Resolution PSs for Wideband mmWave MIMO-OFDM Systems," *IEEE J. Sel. Areas Commun.*, vol. 38, no. 9, pp. 2168–2181, Sept. 2020, DOI: 10.1109/JSAC.2020.3000878.
[24] J. Jiang, Y. Yuan, and L. Zhen, "Multi-User Hybrid Precoding for Dynamic Subarrays in mmWave Massive MIMO Systems," *IEEE Access*, vol. 7, pp. 101718–101728, 2019, DOI: 10.1109/ACCESS.2019.2929927.
[25] J. Jin, C. Xiao, W. Chen, and Y. Wu, "Channel-Statistics-Based Hybrid Precoding for Millimeter-Wave MIMO Systems with Dynamic Subarrays," *IEEE Trans Commun*, vol. 67, no. 6, pp. 3991–4003, June 2019, DOI: 10.1109/TCOMM.2019.2899628.
[26] X. Volker Aue, Dresden, Germany, "The Open RAN System Architecture and m-MIMO," *Microwave Journal*, pp. 70–82, 2021.
[27] Q. H. Spencer, A. L. Swindlehurst and M. Haardt, "Zero-forcing methods for downlink spatial multiplexing in multiuser MIMO channels," *IEEE Trans. Signal Process.*, vol. 52, no. 2, pp. 461–471, Feb. 2004, DOI: 10.1109/TSP.2003.821107.
[28] Q. H. Spencer, C. B. Peel, A. L. Swindlehurst, and M. Haardt, "An introduction to the multi-user MIMO downlink," *IEEE Commun. Mag.*, vol. 42, no. 10, pp. 60–67, Oct. 2004, DOI: 10.1109/MCOM.2004.1341262.
[29] Zukang Shen, Runhua Chen, J. G. Andrews, R. W. Heath, and B. L. Evans, "Low complexity user selection algorithms for multiuser MIMO systems with block diagonalization," *IEEE Trans. Signal Process.*, vol. 54, no. 9, pp. 3658–3663, Sept. 2006, DOI: 10.1109/TSP.2006.879269.
[30] H. Fan, X. Liang, J. Geng, R. Jin, and X. Zhou, "Reconfigurable Unequal Power Divider with a High Dividing Ratio," *IEEE Microw Wirel Compon Lett*, vol. 25, no. 8, pp. 514–516, Aug. 2015, DOI: 10.1109/LMWC.2015.2440774.
[31] H. Ren, M. Zhou, Y. Gu, and B. Arigong, "A Tunable Transmission Line with Controllable Phase Shifting and Characteristic Impedance," *IEEE Trans. Circuits Syst. II: Express Br.*, vol. 67, no. 10, pp. 1720–1724, Oct. 2020, DOI: 10.1109/TCSII.2019.2946307.
[32] H. Fan, X. Liang, J. Geng, L. Liu, and R. Jin, "An N-Way Reconfigurable Power Divider," *IEEE Trans Microw Theory Tech*, vol. 65, no. 11, pp. 4122–4137, Nov. 2017, DOI: 10.1109/TMTT.2017.2702115.
[33] S. Park and R. W. Heath, "Spatial Channel Covariance Estimation for mmWave Hybrid MIMO Architecture," *2016 50th Asilomar Conf. Signals Syst. Comput.*, 2016, pp. 1424–1428, DOI: 10.1109/ACSSC.2016.7869611
[34] 3GPP, "Study on channel model for frequencies from 0.5 to 100 GHz," TR 38.900 Release 14, 2017.
[35] S. Lavdas, P. K. Gkonis, Z. Zinonos, P. Trakadas and L. Sarakis, "An Adaptive Hybrid Beamforming Approach for 5G-MIMO mmWave Wireless Cellular Networks," *IEEE Access*, vol. 9, pp. 127767–127778, 2021, DOI: 10.1109/ACCESS.2021.3112514.

Kai Xu received the bachelor's degree in Telecommunication Engineering (Honours of the First Class) from Xidian University, Xi'an, China, and Heriot-Watt University, Edinburgh, UK, in 2019. The master's degree in Science in Telecommunications (with distinction) from Heriot-Watt University, Edinburgh, UK, in 2020. He is currently pursuing the Ph.D. degree with the Edinburgh Research Partnership in Engineering, Heriot-Watt University and University of Edinburgh, UK.

His primary research interests include Ambient backscatter communication, energy harvesting, Internet of things, hybrid beamforming network for Massive MIMO.

Jiayu Hou received her BEng degree in Telecommunication Engineering from both Heriot-Watt University (Honours of the First Class), UK, and Xidian University, China, in 2022. She is currently pursuing the Ph.D. degree with the Edinburgh Research Partnership in Engineering, Heriot-Watt University and University of Edinburgh, UK. Her research interest focus on power amplifier linearization, massive multiple input multiple output communication system, antenna array, and beamforming network.

Li Wang (Senior Member, IEEE) received the Ph.D. degree from the University of Southampton, Southampton, U.K., in 2010. From 2010 to 2012, he conducted research as a Senior Research Fellow with the School of Electronics and Computer Science, University of Southampton. During his academic period, he was involved in a number of national projects, such as those from UK's EPSRC, Mobile VCE, and Indian–UK Advanced Technology Centre. In March 2012, he joined the R&D Center of Huawei Technologies in Stockholm, Sweden. He is currently working as a senior algorithm expert with Wireless Network Algorithm Lab, Stockholm, Sweden leading a team focusing on 5G PHY/MAC algorithm design. He has been an adjunct professor in UESTC, China and a member of Isaac Newton Institute for Mathematical Sciences, University of Cambridge. He has authored 50+ research papers in IEEE/IET journals and conferences, and also coauthored one JohnWiley/IEEE Press book on LTE. His research interests include both radio transmission technology and radio resource management areas for future wireless communication technologies and networks, including cross-layer cross-module system design, millimeter Wave, communication system intelligentization and sparse/distributed signal processing. He was the recipient of several Huawei awards, including Huawei Individual Contribution Award in 2015, Huawei Furture Star Award in 2017, and Huawei Outstanding Individual Award in 2019 and 2021. His team have been awarded Huawei Team Gold Medal twice in 2018 and 2021, respectively.

Simona Sibio received the B.Eng. and the M.Sc. degrees (Honours) in Electrical and Electronic Engineering in the University of Calabria, in 2016 and 2019, respectively. During her student years, she worked in several projects for digital signal processing within Electronic Research Group of University of Calabria, and as an FPGA designer in the Italian National Agency for New Technologies, Energy, and the Sustainable Economic Development (ENEA). In 2019, she was enrolled as visiting scholar in Heriot-Watt University focusing on a MIMO testbed and Load Pull implementation using USRPs. She is currently pursuing the Ph.D. program in collaboration with Xilinx at Heriot-Watt University. Her research interests include digital signal processing in the new generations of networks, analysis of 5G NR system performance, and digital implementations of beamforming and channel estimation on state-of-art technologies.

John S. Thompson (F'16) received the Ph.D. degree in electrical engineering from University of Edinburgh, Edinburgh, U.K., in 1996. He currently holds a personal chair in Signal Processing and Communications at the School of Engineering, University of Edinburgh. He specializes in antenna array processing, energy-efficient wireless communications and the application of machine learning to wireless communications problems. To date, he has published in excess of 350 papers on these topics. His work has been regularly cited by the wireless community and from 2015 to 2018, he was recognized by Thomson Reuters as a Highly Cited Researcher. He is currently an area editor handling wireless communications topics for the IEEE Transactions on Green Communications and Networking journal. In January 2016, he was elevated to Fellow of the IEEE for Contributions to Antenna Arrays and Multihop Communications.

Stephen McLaughlin (Fellow, IEEE) received the B.Sc. degree from the University of Glasgow, Glasgow, U.K., in 1981 and the Ph.D. degree from the University of Edinburgh, Edinburgh, U.K., in 1990. From 1981 to 1986, he was a Development Engineer with Industry. In 1986, he joined the Department of Electronics and Electrical Engineering with the University of Edinburgh and ultimately held a Chair in Electronic Communication Systems. In October 2011, he joined Heriot-Watt University, Edinburgh, U.K., as a Professor of signal processing. Prof. McLaughlin is a Fellow of the Royal Academy of Engineering, the Royal Society of Edinburgh, the Institute of Engineering and Technology, a EURASIP.

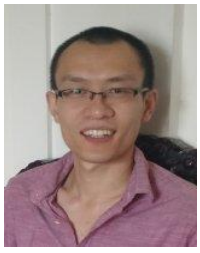

Yuan Ding (Member, IEEE) received the bachelor's degree in electronic engineering from Beihang University, Beijing, China, in 2004, the master's degree in electronic engineering from Tsinghua University, Beijing, in 2007, and the Ph.D. degree in electronic engineering from the Queen's University of Belfast, Belfast, U.K., in 2014. He was a Radio Frequency (RF) Engineer with the Motorola Research and Development Centre, Beijing, from 2007 to 2009, before joining Freescale Semiconductor, Inc., Beijing, as an RF Field Application Engineer, responsible for high-power base-station amplifier design from 2009 to 2011. He is currently an Associate Professor with the Institute of Sensors, Signals and Systems, Heriot-Watt University, Edinburgh, U.K. His research interests are in antenna arrays, physical layer security, and 5G-related areas. Dr. Ding was a recipient of the IET Best Student Paper Award at the Loughborough Antennas and Propagation Conference (LAPC) 2013 and the Young Scientists Awards in the General Assembly and Scientific Symposium, 2014 XXXIst International Union of Radio Science (URSI)

Gunnar Peters is a Senior Expert in Network Algorithms at Huawei Sweden. He has a PhD in Mathematics and Master of Engineering in Applied Physics from the Royal Institute of Technology. He has worked in telecom for 19 years and started at Ericsson 2000 were he was an expert in Radio Performance. In 2010 he joined the Wireless organization at Huawei Sweden, where he is the director of wireless network algorithm lab. Gunnar has also worked at the University of South Carolina, Uppsala University and the Royal Institute of Technology. His research covers stochastic cstate mechanics, signal processing, and radio resource management. Gunnar has received the Individual Gold Medal Award and the Team Gold Medal Award for his work in massive MIMO, advanced receivers and the application of machine learning to RAN.